

## Laboratory study of wind impact on steep unidirectional waves in a long tank

Zhang, Zitan; Tang, Tianning; Zheng, Xiaobo; Xu, Wentao; Zhang, Lijun; Lee, Jung Hoon; Adcock, Thomas A.A.; Monty, Jason P.; Slunyaev, Alexey; Van Den Bremer, Ton S.

**DOI**

[10.1103/PhysRevFluids.9.104801](https://doi.org/10.1103/PhysRevFluids.9.104801)

**Publication date**

2024

**Document Version**

Final published version

**Published in**

Physical Review Fluids

**Citation (APA)**

Zhang, Z., Tang, T., Zheng, X., Xu, W., Zhang, L., Lee, J. H., Adcock, T. A. A., Monty, J. P., Slunyaev, A., Van Den Bremer, T. S., & Li, Y. (2024). Laboratory study of wind impact on steep unidirectional waves in a long tank. *Physical Review Fluids*, 9(10), Article 104801. <https://doi.org/10.1103/PhysRevFluids.9.104801>

**Important note**

To cite this publication, please use the final published version (if applicable).  
Please check the document version above.

**Copyright**

Other than for strictly personal use, it is not permitted to download, forward or distribute the text or part of it, without the consent of the author(s) and/or copyright holder(s), unless the work is under an open content license such as Creative Commons.

**Takedown policy**

Please contact us and provide details if you believe this document breaches copyrights.  
We will remove access to the work immediately and investigate your claim.

***Green Open Access added to TU Delft Institutional Repository***

***'You share, we take care!' - Taverne project***

**<https://www.openaccess.nl/en/you-share-we-take-care>**

Otherwise as indicated in the copyright section: the publisher is the copyright holder of this work and the author uses the Dutch legislation to make this work public.

## Laboratory study of wind impact on steep unidirectional waves in a long tank

Zitan Zhang <sup>1</sup>, Tianning Tang <sup>2</sup>, Xiaobo Zheng <sup>3</sup>, Wentao Xu <sup>1</sup>, Lijun Zhang <sup>1</sup>,  
Jung-hoon Lee <sup>4</sup>, Thomas A. A. Adcock <sup>2</sup>, Jason P. Monty <sup>4</sup>, Alexey Slunyaev <sup>5</sup>,  
Ton S. van den Bremer <sup>2,6</sup> and Ye Li <sup>7,1,8,9,10,\*</sup>

<sup>1</sup>Multifunction Towing Tank Laboratory, *Shanghai Jiao Tong University, Shanghai 200240, China*

<sup>2</sup>Department of Engineering Science, *University of Oxford, Oxford OX1 3PJ, United Kingdom*

<sup>3</sup>College of Energy and Power Engineering, *Lanzhou University of Technology, Lanzhou 730050, China*

<sup>4</sup>Department of Mechanical Engineering, *The University of Melbourne, Victoria 3010, Australia*

<sup>5</sup>Institute of Applied Physics, *Russian Academy of Sciences, Nizhny Novgorod 603950, Russia*

<sup>6</sup>Faculty of Civil Engineering and Geosciences, *Delft University of Technology, 2628 CD Delft, The Netherlands*

<sup>7</sup>Department of Ocean Science and Engineering, *Southern University of Science and Technology, Shenzhen 518055, China*

<sup>8</sup>School of Engineering, *The University of Edinburgh, The King's Buildings, Edinburgh EH9 3JL, United Kingdom*

<sup>9</sup>Department of Civil and Mechanical Engineering, *Technical University of Denmark, Nils Koppels Allé, Kgs 2800 Kgs. Lyngby, Denmark*

<sup>10</sup>Department of Wind and Energy Systems, *Technical University of Denmark, Nils Koppels Allé, Kgs 2800 Kgs. Lyngby, Denmark*



(Received 2 December 2023; accepted 7 August 2024; published 2 October 2024)

Understanding the effect of wind forcing on steep unidirectional waves is important for the study of wind-wave interaction. In this paper, unidirectional random wave experiments are carried out in a large-scale wave tank in which waves interacted with turbulent wind generated by wind fans. The properties and evolution of deep-water gravity waves subject to following wind forcing are investigated through parametric laboratory experiments. The effect of wind forcing on the significant wave height varies with the initial wave steepness. Wind forcing increases the growth of waves of small initial steepness but attenuates large, steep waves as a result of the vertical angle of the wind to the free surface in our experiments. The energy input by wind forcing increases the high-frequency tail of the wave spectra, and this effect increases with fetch. The mean frequency increases under wind forcing. The effect of wind forcing on the probability of extreme events is investigated. Wind forcing enhances wave steepness, resulting in a deviation of the exceedance probability from first-order and second-order theoretical distributions and an increased value of kurtosis but not skewness.

DOI: [10.1103/PhysRevFluids.9.104801](https://doi.org/10.1103/PhysRevFluids.9.104801)

### I. INTRODUCTION

The accurate description of extreme events is the basis for the design of much offshore infrastructure, and effective prediction can improve the safety of operation of these structures [1]. In recent decades, accidents involving floating offshore structures could be related to extreme events

\*Contact author: [liye@sustech.edu.cn](mailto:liye@sustech.edu.cn)

[2], which has prompted scientists and engineers to pursue further research on wave evolution and dynamics [3,4]. With the rapid development of nonlinear dynamics in theory and experiment, different physical mechanisms have been proposed for extreme waves [5], such as dispersive focusing [6], wave-current interaction [7], and nonlinear interaction leading to modulational instability [8,9]. Recently, there has been renewed interest in how wind forcing enhances modulation instability by investigating the effect of wind forcing on a Peregrine breather [10]. It is therefore important to investigate the role of wind-wave interaction in wave evolution and consequent extreme wave generation.

In air-sea interaction, wind is the driving force that generates surface waves. There is an exchange of momentum and energy between the wind and these waves. Here, we focus on the local interaction on a wave-by-wave basis, a different scale from the extensive existing body of work on wind energy transfer at a wave-averaged level in spectral wave models. Wind impact on waves has been studied extensively in the past decades, especially examining wave growth. Although phase-averaged modeling of energy input from wind to waves is relatively mature, the effect of wind on wave evolution on a wave-by-wave basis has received less attention [11], especially after innovative offshore structure booms such as offshore renewables [12–14] and floating islands [15–17]. Three aspects of the wind's impact on waves can be distinguished. First, the pressure at the air-sea interface drives wave motion. Second, wind-induced currents are generated by the tangential shear stress imposed by the wind at the interface. Both the wind's driving force and wind-induced current affect the evolution of wave groups [18]. Third, wind forcing has an impact on modulation instability. Onorato and Proment [19] investigated the effects of wind forcing and dissipation on modulational instability. Brunetti and Kasparian [20] compared the effect of modulation instability in weak and strong wind forcing and suggested that strong wind forcing can enhance modulation instability. Maleewong and Grimshaw [21] developed a modified, fully nonlinear model and compared wave group formation with and without wind forcing. Their results suggested that wind forcing induces an exponential growth rate in the maximum amplitude of waves. In addition, they also observed wave breaking in cases with high wave steepness. Chabchoub *et al.* [22] performed an experimental investigation to study the evolution of Peregrine breathers with wind forcing. Their results suggest that weak wind forcing does not have a significant impact on the evolution of Peregrine breathers but that strong wind does enhance its amplitude. Recently, Toffoli *et al.* [23] presented a set of field observations to reveal the effects of wind forcing and nonlinear interactions on the wave statistics. The results suggest that waves can develop into a strong non-Gaussian process with the wind forcing and the extreme waves frequently generated, leading to the heavy-tailed statistics with non-Gaussian properties.

Table I summarizes the findings of the different numerical simulations and laboratory experiments investigating wind-induced growth and attenuation of waves in recent decades. The effects of wind on wave growth (or attenuation) found in these studies are not consistent on first inspection (cf. two rightmost columns of Table I, which show whether the study reports growth or attenuation of the wave height due to wind). Amplification of wave height is the strongest evidence of wave growth and can be used to evaluate the effect of wind forcing on a dispersively focused wave group. Kharif *et al.* [26] and Touboul *et al.* [41,42] studied wind impact on focused wave groups theoretically and experimentally. Their results suggest that an asymmetric response of wave height amplification between wave focusing and defocusing leads to an enhancement of the duration of extreme wave events. Tian and Choi [27] carried out experiments on unidirectional dispersively focused wave groups with a following wind and compared these with numerical simulations, developing a wind-wave model based on wind-induced currents and wave breaking. Zou and Chen [29] investigated the effects of wind and wind-driven current on wave group evolution using a two-phase flow model. They showed that the airflow separated at the steep wave crest and generated a pressure drop at the leeward side of the wave crest. The form drag induced by the pressure asymmetry significantly affected extreme wave heights, increasing them for following wind and reducing them for opposing wind. In addition, extreme waves enhanced the momentum and energy transfer at the air-water interface [29]. Waseda and Tulin [43] performed a laboratory experiment to investigate the impact of wind on the instability of nonlinear deep-water wave trains. Their results suggest that the growth

TABLE I. Review of previous laboratory experiments (EXP) and numerical simulations (NS) of wind-wave interaction. Numerical methods used are denoted as follows: BIEM (boundary integral equation method), VOF (volume of fluid method), ESBI (enhanced spectral boundary integral method), HOS (high-order spectral method), LES (large-eddy simulation). Wave types are denoted as follows: RW (regular wave), IRW (irregular wave), and DFW (dispersively focused wave). Wind types are denoted as follows: FW (following wind), OW (opposing wind). Here,  $\lambda$  is the characteristic wavelength (the wavelength corresponding to the smallest peak frequency studied in each paper is shown in case multiple peak frequencies are studied),  $d$  is the water depth, 2D denotes a two-dimensional numerical simulation, and wave age is the ratio of the wave phase velocity  $c$  to the instantaneous friction velocity  $u^*$ .

Authors	EXP/NS	Scale ( $L \times W \times d$ )	Wave type	Wind type	Wind speed [min, max] (m/s)	Wave age [min, max]	Growth	Attenuation
Peirson <i>et al.</i> [24]	EXP	$19.23\lambda \times 0.58\lambda \times 0.71\lambda$	IRW	OW	[5, 15]	-	✓	✓
Touboul <i>et al.</i> [25]	NS (BIEM)	$24.64\lambda \times 0.64\lambda$ (2D)	DFW	FW	[4, 6]	-	✓	
Kharif <i>et al.</i> [26]	EXP	$25.64\lambda \times 1.16\lambda \times 0.64\lambda$	DFW	FW	[4, 10]	-	✓	
Tian and Choi [27]	EXP	$11.64\lambda \times 1.16\lambda \times 0.42\lambda$	DFW	FW	[1.4, 5.0]	-	✓	
	NS	$38.79\lambda$ (2D)	DFW	FW	[0.958, 3.832]	-	✓	
Saket <i>et al.</i> [28]	EXP	$53.41\lambda \times 1.07\lambda \times 0.82\lambda$	DFW	FW	[1.4, 2.0]	-	✓	
Zou and Chen [29]	NS (VOF)	$9.43\lambda \times 0.77\lambda$	DFW	OW	[-1.4, -5.0]	-	✓	
				FW	[1.4, 5.0]	-	✓	
Wang <i>et al.</i> [30]	NS (ESBI)	$32\lambda \times 32\lambda$ (2D)	DFW+RW	FW	[6]	[4, 5]	✓	
Hasan <i>et al.</i> [31]	NS (HOS)	$50.86\lambda \times 0.32\lambda$ (2D)	DFW	FW	[2, 8]	-	✓	
Cao <i>et al.</i> [32]	NS (LES)	$6\lambda \times 4\lambda \times 1\lambda$	RW	OW	[-1.4, -5.0]	[0.1, 0.8]	✓	
Lee and Monty [33]	EXP	$38.46\lambda \times 1.15\lambda \times 0.58\lambda$	IRW	FW	[4.8, 13.6]	-	✓	
Cao and Shen [34]	NS (LES)	$6\lambda \times 4\lambda \times 1\lambda$	RW	FW	-	[0.1, 1.4]	✓	
Shemer and Singh [35]	EXP	$4.39\lambda \times 0.35\lambda \times 0.17\lambda$	RW	FW	[5.1, 11.5]	-	✓	
Kristoffersen <i>et al.</i> [36]	EXP	$16.41\lambda \times 1.07\lambda \times 0.37\lambda$	IRW	FW	[5.5, 7.0]	-	✓	
Husain <i>et al.</i> [37]	NS (LES)	$5\lambda \times 5\lambda \times 2.435\lambda$	RW	FW	-	[1.4, 11.0]	✓	
				OW	-	[-1.4, -11.0]	✓	
Georgios <i>et al.</i> [38]	NS	$12\lambda \times 4\lambda \times 1\lambda$	RW	FW	-	[2, 25]	✓	
				OW	-	[-2, -25]	✓	
Chen and Zou [39]	NS (VOF)	$11.64\lambda \times 1.16\lambda \times 0.42\lambda$	DFW	OW	[-1.4, -5.0]	-	✓	
				FW	[1.4, 5.0]	-	✓	
Husain <i>et al.</i> [40]	NS (LES)	$5\lambda \times 5\lambda \times 2.435\lambda$	RW	OW	-	[-1.4]	✓	
				FW	-	[1.4]	✓	
Present paper	EXP	$85.47\lambda \times 4.56\lambda \times 2.14\lambda$	IRW	FW	[8.2]	-	✓	
	NS (LES)	$11.40\lambda \times 0.06\lambda \times 2.14\lambda$	RW	FW	[8.2]	-	✓	

rate of the sidebands decreases with wind forcing but increases in strong wind forcing. It is worth noting that in the laboratory experiments of Kristoffersen *et al.* [36], both the growth and the attenuation of waves were observed in the cases with following wind. Their results suggest that the number of breaking waves increases with wind speed, and the reason for wave attenuation is energy dissipation induced by wave breaking. In contrast to traditional experiments with mechanically generated waves, Toffoli *et al.* [44] investigated the statistical properties of wind-induced waves and the formation of extreme waves in an annular wave flume. Wind-induced waves were generated by a constant and quasi-homogeneous wind blowing over an annular wave flume, allowing the sea state to become fully developed. Significant deviations from Gaussian statistics were observed in the evolution of wind-induced waves. Recently, Lee and Monty [33] performed a laboratory experiment to investigate the impact of wind on an existing random sea. They found that the amplitude modulation of wave groups within this random sea increases with additional wind input, and a theoretical argument for this is given in Adcock and Taylor [45].

An alternative robust method for evaluating wave growth (attenuation) is to use the wave growth (attenuation) rate parameter determined by form drag and wave steepness. Cao *et al.* [32] performed a wall-resolved large-eddy simulation (LES) to investigate the interaction between waves and opposing turbulent wind and developed a viscous model that used nonorthogonal computational coordinates. The slight pressure asymmetry induced by viscous stress plays a crucial role in wave attenuation. The form drag exerted by the turbulent wind on the opposing wave attenuates the wave. On this basis, Cao and Shen [34] investigated the effect of fast-propagating (i.e., faster than the wind speed) water waves on wind and clarified the mechanism through which form drag affects the wavy surface. Their results suggest that there is a threshold for wave age ( $c/u^* = 20$  with  $c$  the wave phase speed and  $u^*$  the friction velocity in the air), where wave growth decreases when wave age is below the threshold (and waves are “young”) and increases when wave age is above the threshold (and waves are “old”).

In summary, wave growth arises mainly due to pressure asymmetry caused by the wind flowing over the waves [25,29,32,34,37–40] and the enhancement of wave modulation by the wind [10,19,20,33,45]. Opposing wind is an important but not the only factor leading to wave attenuation [24,29,37–40]. The growth of extreme waves is limited by wave breaking as the local wave steepness of waves increases with wind speed [33]. Although extensive research on wind-wave interaction has been carried out, the physical mechanism governing the interaction between extreme waves and wind forcing has not been well understood. In experimental studies, the scale of the wave flume typically limits the evolution of waves in the propagation direction and makes it difficult to avoid the effect of boundaries due to the sidewalls in the direction normal to this. Similarly, due to the limitation imposed by computational cost in numerical simulations, regular waves [46] or dispersively focused irregular waves [39] instead of random waves are typically used as input.

In this paper, the effect of wind forcing on the probability of extreme waves is examined by carrying out a laboratory study of random waves subject to wind forcing generated by wind fans in a very large ( $L = 300$  m,  $w = 16$  m,  $d = 7.5$  m) wave tank, with the aim of providing a deeper understanding of wind-wave interaction in complex ocean conditions. Compared with previous wind-wave experiments, the scale of the tank is larger, which ensures the full development of steep unidirectional waves and turbulent wind. In addition, the airflow generated by the mechanical wind fans above our open tank has a higher turbulence intensity (approximately 12%) than previous experiments (e.g., the turbulence intensity is only 0.5% in [33], who use a closed wind-wave tank), which is more similar to values observed in the atmospheric boundary layer [47]. The atmospheric boundary layer is characterized by high turbulence intensities of 10%–20% [48,49]. We take as our starting point as the pioneering deep-water, unidirectional extreme wave experiments by Onorato *et al.* [50] (henceforth O04), which we modify by adding wind generation.

The remainder of this paper is organized as follows. In Sec. II, the setup of the experimental facility is described. The experimental results are given in Sec. III, followed by a detailed discussion of wave growth and attenuation in Sec. IV.

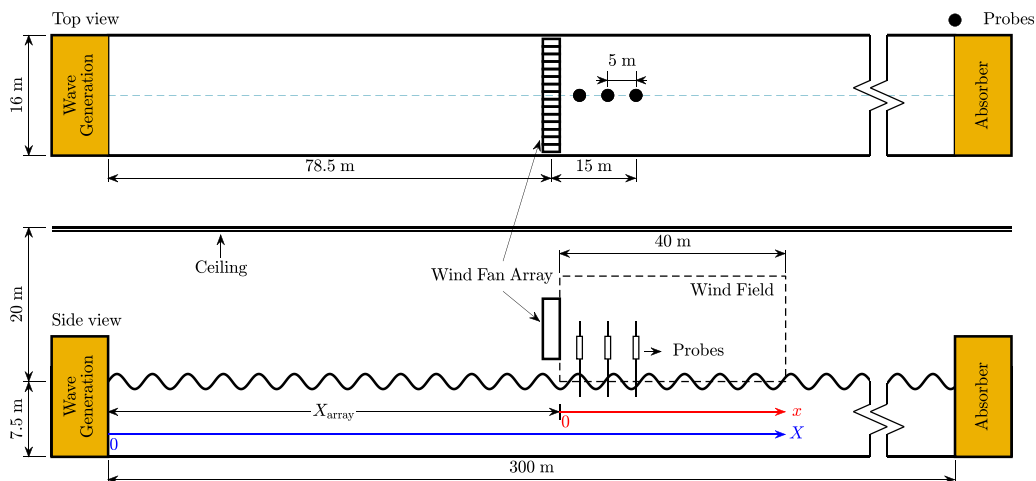


FIG. 1. Diagram of the multifunction towing tank at SJTU and the location of the wind fan array (not to scale).

## II. EXPERIMENTAL SETUP

The laboratory experiments were conducted in the multifunction towing tank at Shanghai Jiao Tong University (SJTU), which has previously been used to study aspects of wave evolution [51–53].

In the equipment design for wind-wave experiments, people must choose between either fully developed waves with a developing wind or a fully developed boundary layer (wind) with developing waves. A typical scenario of wind-wave interaction in the ocean is that waves interact with developing wind in their evolution to form a complex sea state. In this paper, we focus on the effect of wind on (fully developed) wave evolution. Therefore, whether the wave spectrum is in equilibrium when the wave reaches the wind fan array is the basis for the study. We used similar waves as in the pioneering experiments by Onorato *et al.* [50], which are the benchmark for studying extreme waves. On this basis, we designed and installed a fan array to generate the wind forcing.

### A. Facility description

The tank is 300 m in length, 16 m in width, and 7.5 m in maximum depth, as shown in Fig. 1. During the experiment, the working water depth was 7.5 m. There is a 40-paddle hinged-flap-type wave maker at one end of the tank. At the opposite end of the tank a parabolic beach is located. In addition, to reduce the influence of reflected waves, the tank's wave generation system is equipped with active wave absorption and a sidewall wave suppression system.

To study the impact of wind on the wave field, we designed and installed a movable wind fan array above the free surface, as shown in Fig. 2. The array can be installed at designated locations along the 300 m length of the tank. The array consists of 15 accurately calibrated wind fans positioned along a line with their centers 760 mm above the free surface and with a radius of 390 mm each. The maximum working length of the wind over which it is of acceptable quality is 40 m, as shown in Fig. 1. The height of the ceiling above the wind fans is 20 m, and the presence of the ceiling does not affect the wind field. As the characteristics of the wind field are not the main focus of this paper, we include a detailed assessment of the wind field as an appendix (Appendix A).

We use two coordinate systems to distinguish the evolution of the waves (without wind) and the distance of wind-wave interaction. As shown in Fig. 1, the coordinate origin of the wave system (in blue) is the wave maker, and the distance from the wave maker is defined as  $X$ . The distance



FIG. 2. Wind fan array designed and installed in the multifunction towing tank at SJTU.

from the wind fan array is denoted by  $x$  (in red). In our experiments, the wind fan array was set at  $X_{\text{array}} = 78.5$  m. The  $X$  and  $x$  are related by  $x = X - X_{\text{array}}$ .

### B. Experimental conditions

We take as our starting point the pioneering experiment by Onorato *et al.* [50] (henceforth O04), which examined the occurrence of extreme waves in random seas (without wind). Their experimental conditions were previously recreated in the multifunction towing tank at SJTU used in the present study in Tang *et al.* [51] (henceforth T21). O04 used Joint North Sea Wave Project (JONSWAP) spectra with different peak enhancement factors  $\gamma$  to represent different sea states. The fundamental nonlinearity of a sea state, its steepness  $\varepsilon$ , for random deep-water surface gravity waves is defined as

$$\varepsilon = \frac{k_p H_s}{2}, \quad (1)$$

where  $k_p$  is the peak wavenumber and  $H_s$  is the significant wave height. This parameter acts as input for the Benjamin-Feir index [9], which is a ratio of steepness to spectral bandwidth; it acts as a measure of the strength of nonlinear wave-wave interactions and, consequently, of extreme wave prevalence. The Benjamin-Feir index is defined as  $\text{BFI} = \sqrt{2\varepsilon}/(2\nu)$ , where  $\nu = \Delta f/f_p$  is the frequency spectral bandwidth with  $\Delta f$  the half-width at half-maximum and  $f_p$  the frequency at the spectral peak [9]. For broad-banded spectra such as the JONSWAP spectrum, the BFI is most robustly extracted from time series using the method given by Serio *et al.* [54]:

$$\text{BFI} = \sqrt{m_0 k_p Q_p \sqrt{2\pi}}, \quad (2)$$

where  $m_0 = H_s^2/16$  is the zeroth moment of the wave spectrum,  $Q_p$  is the Goda parameter [55], and  $k_p$  is the wavenumber given by the (deep-water) dispersion relation,  $gk_p = \omega_p^2$ , with  $g$  the acceleration due to gravity and  $\omega_p$  the peak wave frequency. The sensitivity of  $Q_p$  to the

TABLE II. Parameters of the laboratory experiments. The experimental parameters of O04 and T21 are reported for reference. We show the input parameters of the experiment and (in square brackets) the parameters measured at the first wave probe (i.e.,  $x/\lambda_{p,0} = 1.4$ , where  $x = 0$  corresponds to the location of the wind fan array and  $\lambda_{p,0}$  is the peak wavelength from the first probe without wind). In the table,  $H_s$  is the significant wave height,  $\gamma$  is the peak enhancement factor,  $\varepsilon$  is the wave steepness,  $\nu$  is the spectral bandwidth,  $Q_p$  is the Goda parameter, and BFI is the Benjamin-Feir index. NW corresponds to the cases without wind forcing and W presents the cases with wind forcing. In the present paper, the wind speed is 8.2 m/s.

Authors	Case		$H_s$ (m)	$\gamma$	$\varepsilon$	$\nu$	$Q_p$	BFI
O04	Case 1		0.11	1.0	0.098	0.28		0.2
	Case 2		0.14	3.3	0.125	0.09		0.9
	Case 3		0.16	6.0	0.142	0.08		1.2
T21	Case 1		0.125	1.0	0.113	0.14	3.88	0.6
	Case 2		0.143	3.3	0.129	0.09	5.92	1.3
	Case 3		0.182	6.0	0.150	0.08	8.68	1.9
Present paper	Case 1	NW	0.11 [0.108]	1.0	0.098 [0.100]	0.289	[4.49]	0.24 [0.55]
		W	0.11 [0.113]	1.0	0.098 [0.105]	0.289	[4.59]	0.24 [0.57]
	Case 2	NW	0.14 [0.144]	3.3	0.125 [0.129]	0.090	[6.48]	0.98 [1.04]
		W	0.14 [0.122]	3.3	0.125 [0.111]	0.090	[6.69]	0.98 [0.97]
	Case 3	NW	0.16 [0.158]	6.0	0.134 [0.137]	0.075	[7.51]	1.26 [1.29]
		W	0.16 [0.144]	6.0	0.134 [0.130]	0.075	[8.06]	1.26 [1.30]

high-frequency tail of the spectrum is lower than that of other bandwidth metrics; it is a dimensionless parameter to measuring the spectral bandwidth [54,56] and can be computed as

$$Q_p = \frac{2}{m_0^2} \int_0^\infty f S^2(f) df, \quad (3)$$

where  $S(f)$  is the energy density spectrum.

We consider three distinct experimental cases with different peak enhancement factors corresponding to the three experiments of O04. Compared to the experiments of O04, we obtain a larger BFI from our time series. We note that the value of BFI strongly depends on the calculation method of bandwidth (see also the discussion in T21). We measured 15 m downstream of the wind fan array (approximately four peak wavelengths) in the mean wave direction (see Fig. 1 for details). Here, we focus on the effect of wind on wave nonlinearity at short distances.

We have repeated each case a total of three times with a new random seed generated in each instance. The wave duration in each experiment was 32 min, and the first 100 s in each time series was deleted in our analysis. This time duration was calculated as the approximate time needed for the wave of twice the peak frequency to reach the last probe. Three capacitance wire wave probes (see Fig. 1 for their locations) with a sampling frequency of 100 Hz were used to measure surface elevation. The wave parameters in the experiments are listed in Table II. The wave peak period  $T_p$  in our experiments is 1.5 s and the duration of the wind forcing is 32 min. The wind fans are run for at least 10 min before wave generation and data acquisition, which ensures that the wind-generated waves in the tank are statistically stable. In our experiments, the wind speed at the center of the fan is 8.2 m/s, measured using an ultrasonic wind speed indicator. The turbulence intensity of the wind is 11%–12%. See Appendix A for measured vertical profiles of the wind velocity.

### III. RESULTS

In this section, we examine the properties of the wave field with and without the effect of wind, considering the effect of wind on wave statistics (Sec. III A), the evolution of wave spectra

(Sec. III B), and extreme value distributions (Sec. III C). The experimental results are summarized in tabular form in Tables V and VI in Appendix C.

Due to linear (viscous dissipation, generation of directionality due to the walls) and nonlinear (nonlinear wave-wave interactions) mechanisms, the statistical properties of the free surface change as the waves propagate down the tank, as most evident from the build up of the high-frequency tail of the spectrum. Whether the spectrum is already in equilibrium when waves reach the fan array or is still undergoing change will be important for studying the interaction between wind and waves. In T21, who used equivalent input spectra in the same experimental facility, the spectrum has reached its equilibrium at the location of the wind fan array ( $X_{\text{array}}/\lambda_{p,0} = 22.4$ , where  $\lambda_{p,0}$  is the peak wavelength at the first probe in the case without wind) chosen in the present study.

### A. Statistical properties of the surface elevation

To evaluate the effect of wind forcing, we define an operator,

$$\Delta A = A_W - A_{NW}, \quad (4)$$

where  $A_W$  represents the value of parameter  $A$  with wind forcing and  $A_{NW}$  the value without wind forcing. Below, we will examine the significant wave height  $H_s$ , steepness  $\epsilon$ , peak wavenumber  $k_p$ , skewness  $\lambda_3$ , and kurtosis  $\lambda_4$ .

We normalize the horizontal distance from the wind fan array  $x$  by the peak wavelength  $\lambda_{p,0}$ , which we always obtain from the wave spectrum at the first probe in the case without wind. We use the linear dispersion relationship to obtain  $\lambda_{p,0}$  from  $f_{p,0}$ , where the subscript 0 denotes the first probe in the case without wind.

#### 1. Significant wave height $H_s$ , peak wavenumber $k_p$ , and steepness $\epsilon$

In Fig. 3(a), we show the variation of the significant wave height along the tank without wind forcing. Error bars show the 95% confidence interval based on the standard deviation. We show the input values (represented by different colored lines) of significant wave height in the experiment for reference. The significant wave height measured is consistent with that input to the wave maker. In addition,  $H_s$  is stable for each case and does not change with distance from the wind fan array  $x$ . Next, Fig. 3(b) shows the spatial evolution of the relative change in  $H_s$  due to wind forcing. For case 1, which has the smallest BFI,  $H_s$  increases slightly after the introduction of wind forcing, as we expect. Surprisingly, for cases 2 and 3, the significant wave height decreased significantly, by 6%–8%. In principle, this could be caused by wave breaking. To further examine the potential effect of wave breaking on the cases with large BFI, we also consider the steepness of the waves. As shown in Fig. 3(c), steepness increases with BFI for the cases without wind forcing. Note that the steepness  $\epsilon$  is calculated as the product of the peak wavenumber  $k_p$  and half the significant wave height  $H_s$  (i.e.,  $\epsilon = k_p H_s$ ). In Fig. 3(d), wave steepness increases in case 1 but reduces in cases 2 and 3. Figure 3(e) shows the variation of the peak wavenumber along the tank without wind forcing. The result suggests that the wavenumber decreases with the fetch increases due to the resonant four-wave interactions. In Fig. 3(f), the wavenumber slightly increases with the wind forcing. Although we did not find that wind promotes wave breaking, we emphasize that breaking stills occurs occasionally in all experiments due to the random nature of the waves.

We consider that the reason for the attenuation of large-BFI waves found in our experiments is related to the structure of the wind generated by the fan array. Due to the absence of a device for airflow straightening, the wind's mean direction is at an angle to the water surface, having both vertical and horizontal components. The effect of the vertical wind on the surface is non-negligible compared with the horizontal wind speed and may attenuate the waves. Therefore, it is highly conceivable that the significant wave height decreases due to the suppression of the waves by the vertical wind. For case 1, the suppression is not significant because the individual crests are still too far (vertically) from the fan outlet, and the significant wave height still increases due to the horizontal wind component.

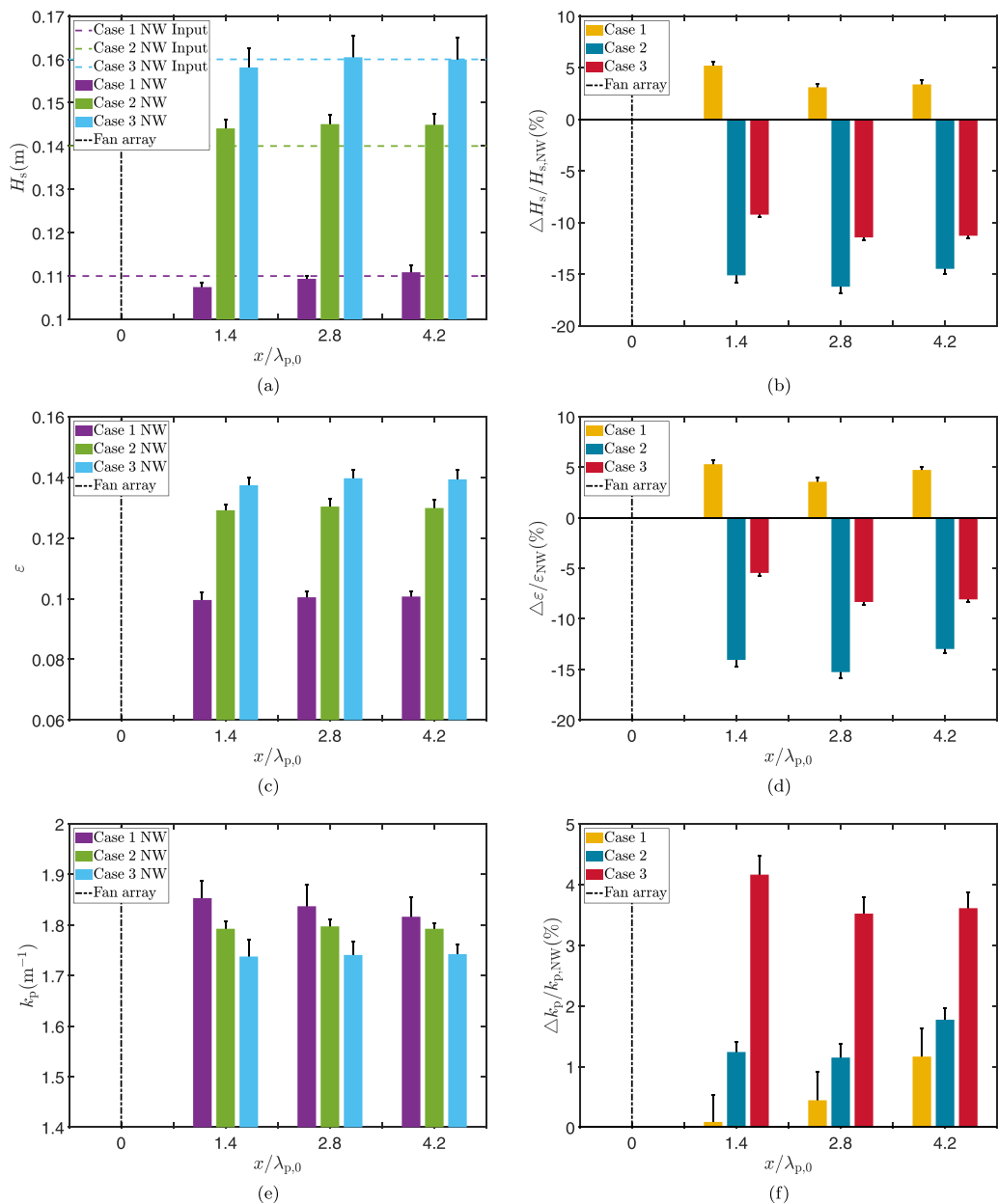


FIG. 3. Effect of wind on (a),(b) significant wave height  $H_s$ , (c),(d) steepness  $\epsilon$ , and (e),(f) peak wavenumber  $k_p$  for three cases with increasing BFI. The left panels show the case without wind (NW), and the right panels show the percentage increase of the three parameters due to wind. Error bars show the 95% confidence interval based on the standard deviation.

To further examine the effect of wind on the significant wave height, we use LESs. See Appendix B for details. LESs have played an increasingly important role in turbulent wind-wave interaction due to their high fidelity. Compared to direct numerical simulations (DNSs), LESs can describe small-scale turbulence without excessive demands on computational power. Because the computational requirements remain very significant even for LESs, we selected regular waves

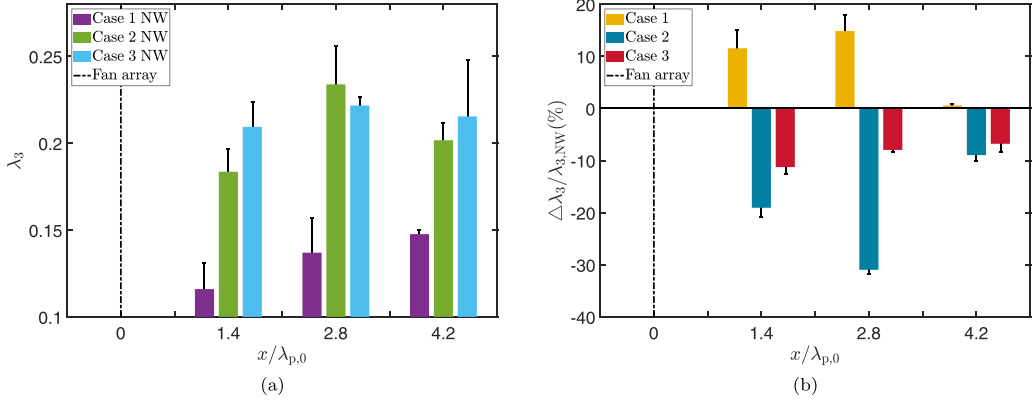


FIG. 4. Effect of wind on skewness  $\lambda_3$  for three cases with increasing BFI. The left panels show the case without wind (NW) and the right panels show the percentage increase due to wind. Error bars show the 95% confidence interval based on the standard deviation.

instead of the irregular waves used in the experiment to qualitatively study the effects of wind on the significant wave height. We used a high-turbulence wind to shear the wavy surface, consistent with the experiment. In the results of the simulations (case 2 NS and case 3 NS) we also observe wave height suppression in case 2 and case 3. We find that the airflow at low fetches is not streamlined due to the insufficient development of the high-turbulence airflow at low fetches; the boundary layer has not adapted to the wavy surface, which leads to wave height suppression by the wind.

## 2. Skewness $\lambda_3$ and kurtosis $\lambda_4$

Skewness and kurtosis are calculated from the measured free surface according to

$$\lambda_3 = \frac{1}{\eta_{\text{rms}}^3} \frac{1}{N} \sum_{n=1}^N (\eta_n - \bar{\eta})^3 \quad \text{and} \quad \lambda_4 = \frac{1}{\eta_{\text{rms}}^4} \frac{1}{N} \sum_{n=1}^N (\eta_n - \bar{\eta})^4, \quad (5)$$

where  $\eta_n$  is the surface elevation at discrete sampling times,  $\bar{\eta}$  is the mean surface elevation,  $\eta_{\text{rms}}$  is the root mean square of the surface elevation, and  $N$  is the length of the signal.

In Fig. 4(a), we show the skewness at different distances from the wind fan array. The positive skewness is typical for water waves, corresponding to sharper crests and flatter troughs caused by second-order bound waves. Figure 4(b) shows the spatial evolution of the difference in skewness due to wind forcing. For cases with large BFI (case 2 and case 3), the skewness decreases, due to the suppression of the wave height by the vertical component of the wind (see above). For case 1, the skewness increases considerably, and the increase in skewness gradually decreases with fetch.

The evolution of kurtosis without wind forcing along dimensionless fetch is shown in Fig. 5(a). The kurtosis of the free surface is greater than 3 (the value for a Gaussian state), indicating that the free surface no longer follows the Gaussian distribution predicted by linear theory, as expected for the nonlinear unidirectional surface gravity waves considered here. The BFI is determined by the steepness of the wave and the spectral width; BFI is known to have an important influence on kurtosis in unidirectional waves [57]. In deep-water, unidirectional waves with larger steepness and more narrow-banded spectra and thus a larger value of BFI, the waves, which all have a value of kurtosis equal to 3 at the wave maker, reach a higher value of kurtosis at distance from the wave maker. The kurtosis reaches its maximum value between 20 and 30 wavelengths from the wave maker, which is consistent with previous results [51,58]. For cases with smaller BFI (case 1 NW), kurtosis is almost constant, with an average value of 3.2. Generally, the increase in kurtosis is significantly dependent on BFI. The kurtosis of the waves increases further due to wind forcing, as

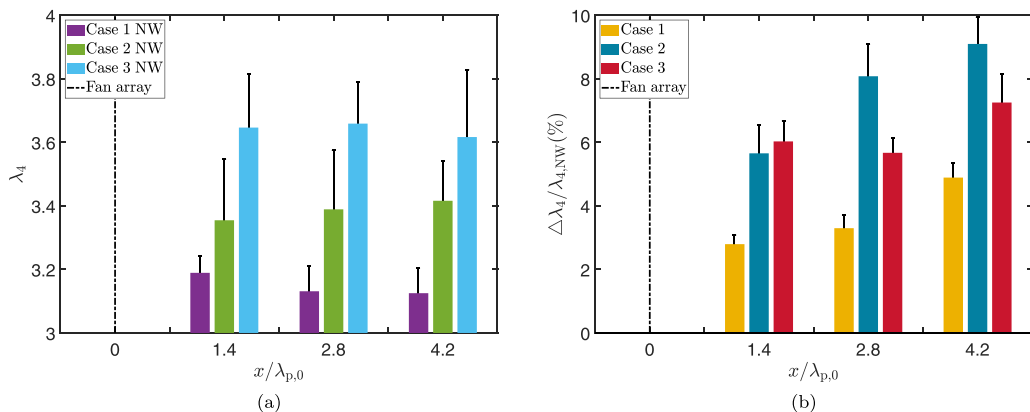


FIG. 5. Effect of wind on kurtosis  $\lambda_4$  for three cases with increasing BFI. The left panels show the case without wind (NW), and the right panels show the percentage increase due to wind. Error bars show the 95% confidence interval based on the standard deviation.

shown in Fig. 5(b). Furthermore, we found that kurtosis increases more significantly due to wind in cases with larger BFI, although not all variation is significant, as is evident from the error bars. This suggests that the likelihood of extreme waves is increased despite the reduction in significant wave height for the higher-BFI cases.

### B. Evolution of wave spectra

During wave evolution, nonlinearity causes wave energy to be redistributed across the spectrum. If the waves become very steep, breaking leads to wave energy dissipation. In Fig. 6, we show the wave spectra with and without wind forcing on a logarithmic scale at the three different dimensionless positions  $x/\lambda_{p,0} = 1.4$ ,  $x/\lambda_{p,0} = 2.8$ , and  $x/\lambda_{p,0} = 4.2$  for the different BFI cases, where  $x$  is the distance from the wind fan array and  $\lambda_{p,0}$  is the peak wavelength from the first probe without wind. First, we focus on the cases without wind forcing (dashed lines in the figure). In all three cases, only a negligible amount of dissipation occurs during the short distance of wave evolution, and the total energy of the waves is constant. No change in the spectrum occurs over the distance shown ( $x/\lambda_{p,0} = 1.4$  to  $x/\lambda_{p,0} = 4.2$ ), confirming that the spectrum is in equilibrium. Upon introduction of the wind (continuous lines), the energy exchange between the wave and the

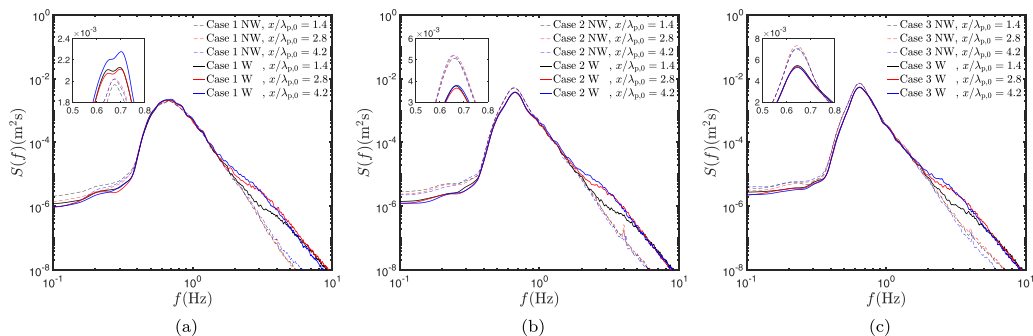


FIG. 6. Spectral evolution with (W) and without (NW) wind forcing: (a) case 1 NW and case 1 W; (b) case 2 NW and case 2 W; (c) case 3 NW and case 3 W.

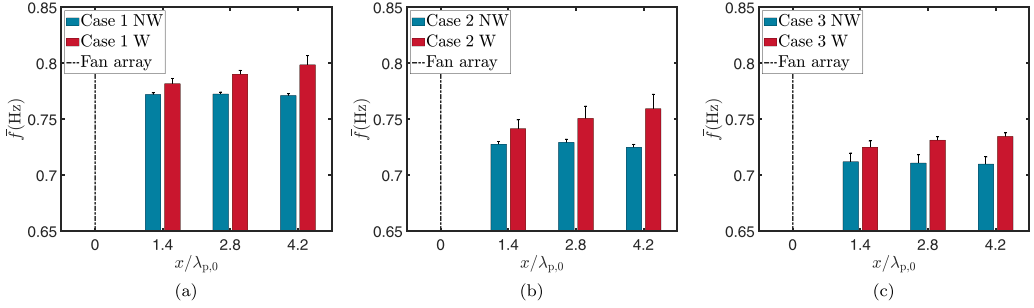


FIG. 7. Evolution of mean frequency with (W) and without (NW) wind forcing: (a) case 1 NW and case 1 W; (b) case 2 NW and case 2 W; (c) case 3 NW and case 3 W. Error bars show the 95% confidence interval based on the standard deviation.

high-speed airflow causes the high-frequency tail of the spectrum to be increased. The growth of the tail increases with fetch and appears to have reached an equilibrium at the final probe ( $x/\lambda_{p,0} = 4.2$ ).

The significant wave height examined above is obtained by calculating the zeroth-order moment of the wave spectrum. In Fig. 6(a), the magnitude of the spectral peak has increased, which is consistent with the increase of the significant wave height due to the wind observed for this case. The magnitude of the spectral peak decreases significantly for cases with a large initial wave height and steepness (and thus a large BFI), as shown in Figs. 6(b) and 6(c), corresponding to the decrease in significant wave height due to the wind observed for these cases. At large enough fetch, we observe a small but significant upshift of the frequency of the spectral peak in all three cases [cf. Fig. 3(f)]. This is different from the suggestion by Hara and Mei [59] that the peak frequency downshifts with the increase of wind forcing. We consider that the nonlinear process of wind-wave interaction does not fully develop in a short distance. Therefore, there is not a significant downshift in the mean frequency. In addition, we consider that wave breaking plays an important role in the evolution of the spectrum. The wave breaking limits the growth of waves and has a negative impact on the statistical results.

To further study the impact of the wind on the wave spectra, we investigate the variation of the mean frequency  $\bar{f}$ . Compared with the peak frequency  $f_p$ , the mean  $\bar{f}$ , an integral quantity, is less affected by fluctuations of the wave spectrum estimated from experiments and therefore more robust [35]. The mean frequency  $\bar{f}$  is determined by the moments of the spectrum. For a discrete power spectrum  $F(f_n)$ , the moments are defined as

$$m_j = \sum_{f_{\min}}^{f_{\max}} f^j F(f_j). \quad (6)$$

Here  $f_{\min}$  and  $f_{\max}$  denote the limits of the spectral domain. The mean frequency  $\bar{f}$  is then given by

$$\bar{f} = \frac{m_1}{m_0}. \quad (7)$$

Figure 7 shows the evolution of the mean frequency with and without wind forcing for unidirectional waves. As in all cases without wind forcing, the mean frequency downshifts with fetch due to wave nonlinearity, but appears to have reached an equilibrium at the start of the wind fan array. Compared to the cases without wind forcing, we found an upshift of the mean frequency due to wind forcing, and the upshifting increases somewhat with fetch. We consider that the main reason for the increase in mean frequency is that the upper tail of the spectrum absorbs the energy from the wind in the wind-wave interaction. To sum up, we note that the mean frequency upshift

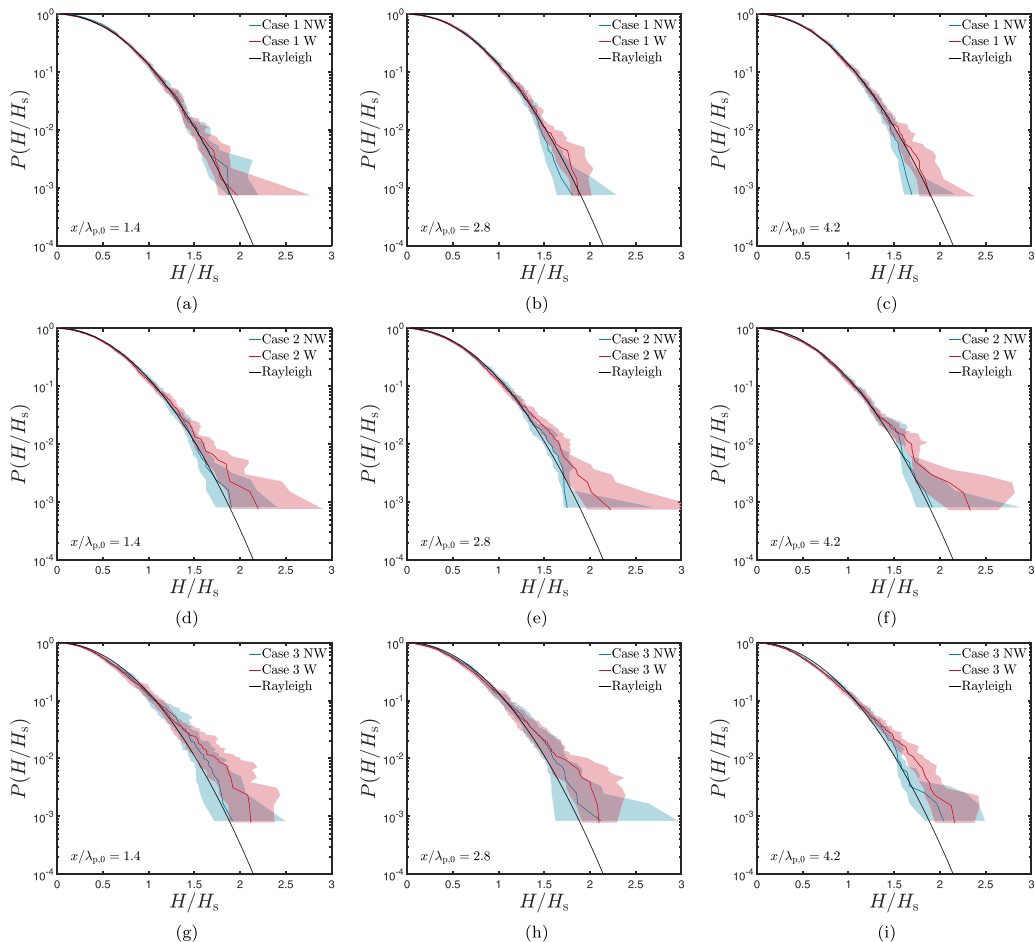


FIG. 8. Comparison between the exceedance probability of wave height  $H$  with (W) and without (NW) wind forcing at different locations, also showing the Rayleigh distribution: (a),(d),(g)  $x/\lambda_{p,0} = 1.4$ ; (b),(e),(h)  $x/\lambda_{p,0} = 2.8$ ; (c),(f),(i)  $x/\lambda_{p,0} = 4.2$  for (a)–(c) case 1; (d)–(f) case 2; (g)–(i) case 3. The shaded regions correspond to 95% confidence intervals based on the bootstrap method.

occurs for all values of BFI despite the reduction in significant wave height for the two larger BFI cases.

### C. Exceedance probability

#### 1. Wave height

Figure 8 shows the exceedance probabilities of wave height  $H$  at the three different locations ( $x/\lambda_{p,0} = 1.4$ ,  $x/\lambda_{p,0} = 2.8$ , and  $x/\lambda_{p,0} = 4.2$ ) with and without wind for cases 1–3. It is difficult to discern a significant deviation from the Rayleigh distribution for the case without wind. Of course, we are interested in the impact of the wind. For case 1, the wind appears to weakly increase the probability of large wave heights at the second probe ( $x/\lambda_{p,0} = 2.8$ ) and third probe ( $x/\lambda_{p,0} = 4.2$ ), but this effect is hardly significant, as shown in Figs. 8(b) and 8(c).

For cases 2 and 3, which have enhanced nonlinearity and BFI compared to case 1, Figs. 8(d)–8(f) and 8(g)–8(i), show that the tail begins to deviate more from the Rayleigh distribution under the influence of wind, and this effect becomes more significant. In other words, extreme events become

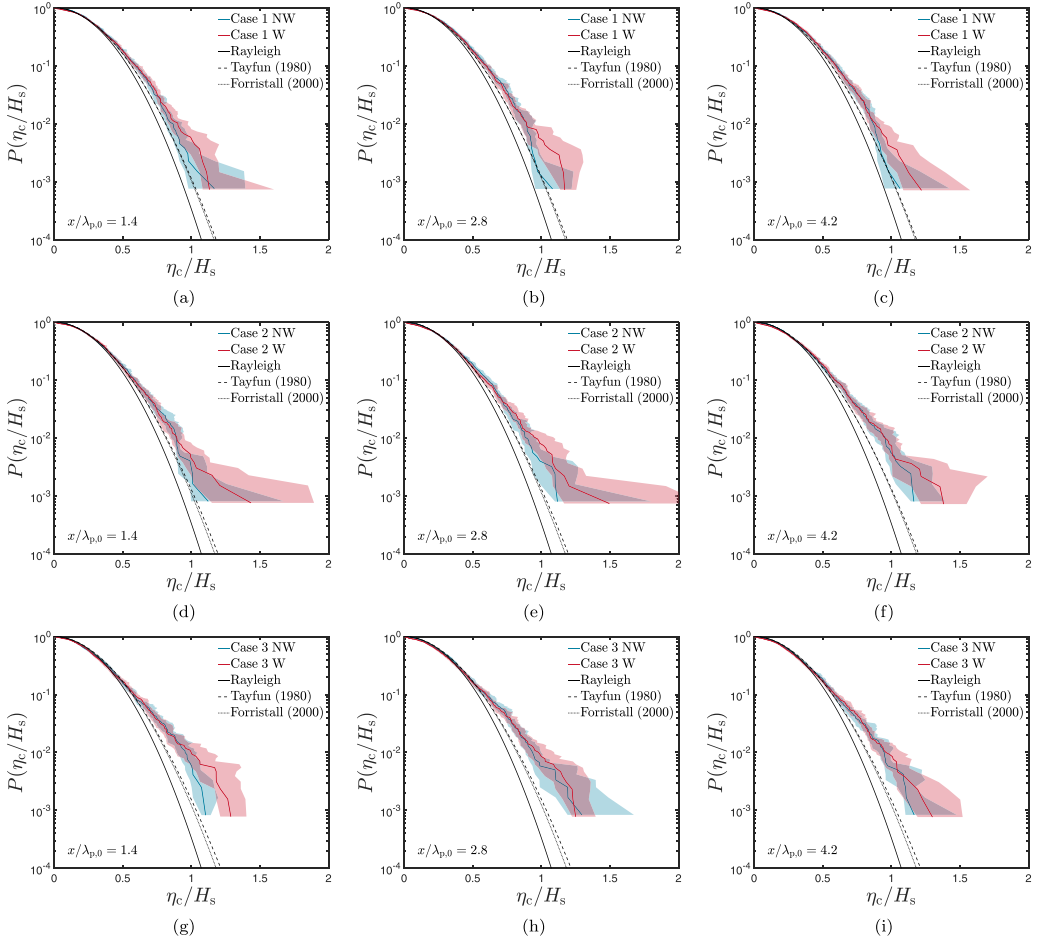


FIG. 9. Comparison between the exceedance probability of crest amplitude  $\eta_c$  with (W) and without (NW) wind forcing at different locations, also showing the Rayleigh, Tayfun, and Forristall distributions: (a),(d),(g)  $x/\lambda_{p,0} = 1.4$ ; (b),(e),(h)  $x/\lambda_{p,0} = 2.8$ ; (c),(f),(i)  $x/\lambda_{p,0} = 4.2$  for (a)–(c) case 1; (d)–(f) case 2; (g)–(i) case 3. The shaded regions correspond to 95% confidence intervals based on the bootstrap method.

more frequent in steep sea states because of wind, despite the reduction in significant wave height observed for these cases in our experiments. The increase in case 3 is not necessarily greater than in case 2, suggesting some kind of saturation. We emphasize the limited significance levels in the tail. It is worth noting that the confidence interval for the exceedance probability increases with  $H/H_s$  increases because the number of rogue waves sampled is small.

## 2. Crest amplitude

Figure 9 compares cases 1–3 with and without the wind forcing to investigate the impact of wind on the crest amplitude distribution. For case 1, the crest amplitude distribution with wind forcing is close to the second-order Tayfun distribution [60]. The results of the Forristall distribution [61] and the Tayfun distribution [60] are almost identical. The BFI of case 1 is small, suggesting only minor effects of (third-order) modulational instability and thus agreement with the second-order distributions of Forristall [61] and Tayfun [60]. The input of wind energy leads to the growth of the tail of the crest amplitude distribution. For case 2, BFI = 0.98 is close to 1 (BFI = 1 is considered as

a threshold above which modulation instability becomes important). Therefore, the crest amplitude distribution is expected to deviate from the Tayfun distribution. After the introduction of wind forcing, the crest amplitude distribution shows a similar increase as in case 1, and the effect is somewhat larger than in case 1. For case 3, the wind forcing increases the wave crest amplitude, but the crest amplitude growth due to the wind decreases with fetch, suggesting some kind of saturation. Again, we emphasize the limited significance levels in the tail. In addition, the uncertainty range of the exceedance probability increases in the tail due to the decrease in the number of rogue waves sampled.

#### IV. DISCUSSION

The goal of this paper has been to study the impact of wind on unidirectional waves. Specifically, we have focused on the exceedance probability of extreme events, which is important for offshore engineering and, for example, the safety of supercarriers. Therefore, unidirectional random wave experiments were carried out in the multifunction towing tank at Shanghai Jiao Tong University. Compared with previous studies, we consider realistic levels of turbulence intensity of the wind and specific attention to the impact of the wind on wave evolution because the wind is one of the causes of extreme events.

In the present work, we have observed that the effect of wind forcing on the significant wave height of waves with different initial wave steepness is different. On the one hand, wind forcing can lead to the growth of waves. Specifically, the significant wave height of cases with small initial steepness increased under the effect of wind forcing (case 1). On the other hand, a decrease in significant wave height due to wind forcing was observed in waves with large initial steepness (cases 2 and 3).

For case 1, our findings of a slight increase in significant wave height due to wind forcing for low initial steepness are consistent with previous experimental studies [24,33]. Airflow separates on the leeward side of the wave crest and results in a pressure drop over the wave crest [29]. This pressure asymmetry produces wave growth [32]. In our spectral analysis, the growth of the high-frequency tail of the wave spectrum, corresponding to the generation of short waves, provides evidence of the transfer of energy from the wind to the waves, and this is consistent with the experimental results of Lee and Monty [33].

For case 1, we have also examined the effect of wind on wave nonlinearity (steepness) and the probability of extreme waves. Steepness increased by a small amount due to wind. The increase of skewness under the effect of wind forcing indicates that the wind increases the asymmetry between the wave crest and the wave trough [62], but this effect decreased with fetch in our experiments. We found that kurtosis increases under the effect of wind forcing, which corresponds to an increase in the probability of extreme events. Therefore, the wind input increases the probability of extreme waves for low initial steepness waves.

However, in cases 2 and 3, the wind forcing produced wave attenuation in contrast with case 1. The significant wave height decreases under the effect of wind forcing. We consider that this wave attenuation is due to the absence of a device for airflow straightening in our experiment and the resulting vertical impact of the mean wind on the wavy surface. In previous experiments, the wind forcing generated by mechanical fans blew horizontally over the waves [26,27,33]. However, the wind generated in our experiment shears the free surface at a certain angle. Therefore, the effect of wind on the wavy surface is more complex. We consider that the vertical component of the wind provides a downward forcing on the wavy surface, producing wave attenuation. This is also observed in large-eddy simulations we have performed to test this hypothesis. The mean frequency of waves increased with fetch under the effect of wind forcing, which corresponds to short waves being generated by the wind-wave interaction. Despite the differences in the effect on significant wave height and steepness, the effect of wind forcing on the probability of extreme waves in cases 2 and 3 is consistent with case 1. Wind forcing increases the probability of extreme events.

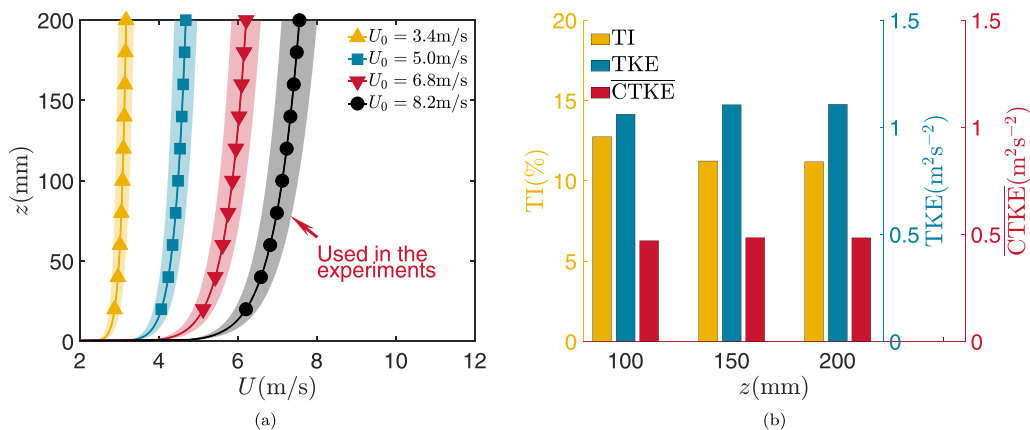


FIG. 10. Calibration of the wind field. (a) Vertical mean wind velocity profiles as a function of distance above the still-water surface (i.e.,  $z = 0$ ) at the first probe (i.e.,  $x/\lambda_{p,0} = 1.4$ ), where  $U_0$  is the wind speed at the center of the fan. The wind profile is fitted well by a power law. The shaded bands of different colors show the 95% confidence intervals of wind speed. (b) Histograms of TI, TKE, and  $\overline{\text{CTKE}}$ .

There are several limitations to our experimental study. In our experiment, the wind-wave interaction occurs within 40 m downstream from the wind fan array (approximately 11 peak wavelengths). However, the wave nonlinearity induced by wind input may not fully develop in a short distance. Onorato *et al.* [50] suggest that it is necessary for 15–20 wavelengths to develop strong non-Gaussian behavior in sea states. Therefore, we need to optimize the setup in the following experiment. We consider increasing the measurement range or reducing the characteristic wavelength to ensure the full development of nonlinear processes. In addition, wave propagation in the ocean is multidirectional and not unidirectional, as considered here. The directional propagation of waves is a key factor affecting the nonlinear physics, which should not be ignored [63]. In addition, the work of Latheef *et al.* [64] and Karpadakis *et al.* [65] shows that the competing mechanisms of nonlinear amplification and wave breaking have a profound impact on crest amplitude statistics. Wave breaking is common in our experiments, even in the case without wind.

In future work, we will focus on the effects of wind gusts on wave evolution. The impact of wind gusts on nonlinear wave growth may be significant [66].

## ACKNOWLEDGMENTS

This research is funded by the National Key R&D Program of China (2023YFB4203303). X.Z. is also funded by National Natural Science Foundation of China (Grant No. 12302298), Science and Technology Program of Gansu Province of China (No. 22JR5RA304). Y.L.’s professorship at DTU is supported by the Otto Mønstedts Foundation.

## APPENDIX A: CALIBRATION OF THE EXPERIMENT

### 1. Wind generation

In the experiment, the wind fan array is installed at  $X = 78.5$  m downstream from the location of wave generation. The wind fan array can generate different wind speeds. Figure 10(a) shows the vertical average wind speed as a function of the distance above the still-water surface at the first probe (i.e.,  $x/\lambda_{p,0} = 1.4$ , which follows well. To maintain a high-quality wind profile, we also control the turbulence level and its structure. We first consider the turbulence intensity, which can be obtained from the three components of the velocity field, which is first decomposed into a mean

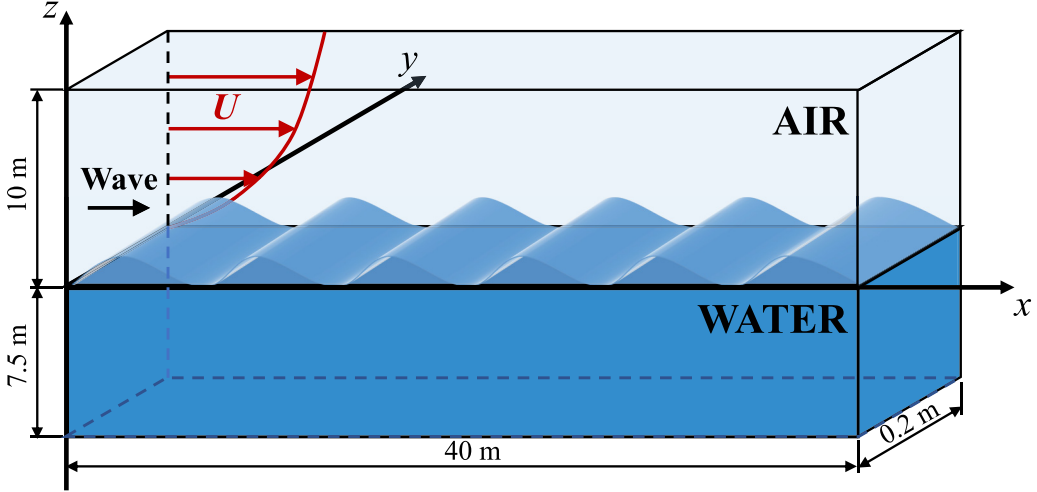


FIG. 11. Diagram of the computational domain used for the large-eddy simulations. The turbulent wind field is driven by the velocity profile  $U(z)$  above the wavy surface. The surface waves propagate in the  $x$  direction.

$\bar{\mathbf{u}}$  and a turbulent perturbation  $\mathbf{u}'$ :

$$\mathbf{u} = \bar{\mathbf{u}} + \mathbf{u}', \quad (\text{A1})$$

where  $\mathbf{u} = u\mathbf{i} + v\mathbf{j} + w\mathbf{k}$ . The horizontal velocities are defined so that  $u$  is aligned with the direction of wave propagation,  $v$  is perpendicular to this in the horizontal plane, and  $w$  is in the upward vertical direction. We report the turbulence intensity (TI), the turbulent kinetic energy (TKE), and the coherent turbulent kinetic energy (CTKE) at the first probe [i.e.,  $x/\lambda_{p,0} = 1.4$ , as shown in Figure 10(b)]. TI, TKE, and CTKE are defined by

$$\begin{aligned} \text{TI} &= \frac{\sigma_u}{\bar{u}}, \\ \text{TKE} &= \frac{1}{2}(\overline{u'^2} + \overline{v'^2} + \overline{w'^2}), \\ \text{CTKE} &= \frac{1}{2}\sqrt{\overline{(u'v')^2} + \overline{(u'w')^2} + \overline{(v'w')^2}}, \end{aligned} \quad (\text{A2})$$

where  $\sigma_u$  is the standard deviation of a 10-min segment and the overline indicates a 10-min average. Results are shown in Figs. 10(a) and 10(b). They show that the wind profile is comparable to a realistic ocean-atmosphere boundary layer [67].

## 2. Wave generation

The elevation of random waves is synthesized as the sum of independent harmonic components, which can be calculated as

$$\eta(t) = \sum_{i=1}^N a_i \cos(2\pi f_i t + \phi_i), \quad (\text{A3})$$

where  $a_i = \sqrt{2S(f_i)\Delta f}$  is the free wave component with  $i$ th frequency  $f_i$  and phase  $\phi_i$ ,  $\Delta f$  is the frequency domain sampling interval, and the phase  $\phi_i$  is sampled from a uniform distribution on  $[0, 2\pi]$ . In this experiment, the target wave spectrum used is the JONSWAP spectrum, which is

TABLE III. Overview of the different numerical simulations.

Case		$H$ (m)	$\varepsilon$	Wind? (Y/N)
Case 1 NS	NW	0.11	0.098	N
	W	0.11	0.098	Y
Case 2 NS	NW	0.14	0.125	N
	W	0.14	0.125	Y
Case 3 NS	NW	0.16	0.134	N
	W	0.16	0.134	Y

given by

$$S(f) = \frac{aH_s^2 f_p^4}{f^5} \exp^{-[1.25(f_p/f)^4]} \gamma \exp^{-1(f-f_p)^2/2\sigma^2 f_p^2},$$

$$a = \frac{0.0624}{0.230 + 0.0336\gamma - \frac{0.185}{1.9+\gamma}}, \quad (\text{A4})$$

where  $\sigma = 0.07$  if  $f \leq f_p$  and  $\sigma = 0.09$  if  $f \geq f_p$ ,  $H_s$  is the significant wave height,  $f_p$  is the spectral peak frequency, and  $\gamma$  is the peak enhancement factor. In this experiment, the peak enhancement factors  $\gamma$  of the spectrum are 1, 3.3, and 6 for cases 1–3, respectively.

### APPENDIX B: NUMERICAL SIMULATIONS

We used LESs to study the turbulent wind-wave interaction because of their high fidelity. The difference from our laboratory experiments is that we use regular waves in the numerical simulations to replace the irregular waves based on the JONSWAP spectrum used in the experiments. Regular waves are chosen to minimize computational time and cost, which are already very significant.

Apart from the difference in the type of waves, the other properties of the numerical simulations are chosen to mimic those of the experiments as closely as possible. The configuration of the three-dimensional numerical tank is shown in Fig. 11. The length of the tank is 40 m, and the height of

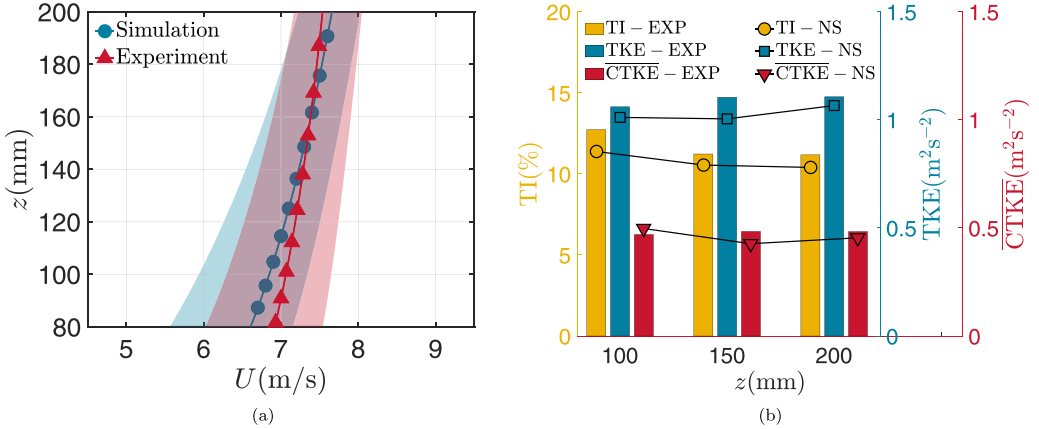


FIG. 12. Comparison of the wind field between numerical simulations (NS) and laboratory experiments (EXP). (a) Vertical mean wind velocity profiles with 95% confidence interval. (b) Histogram of TI, TKE, and CTKE.

TABLE IV. Relative errors of wind parameters between numerical simulations and laboratory experiments.

$z$ (mm)	Wind speed (%)	TI (%)	TKE (%)	$\overline{\text{CTKE}}$ (%)
100	1.60	<b>10.60</b>	4.60	5.94
150	0.35	6.08	<b>9.03</b>	<b>11.72</b>
200	<b>3.04</b>	6.93	3.67	5.95

the computational domain is 17.5 m (7.5 m of water and 10 m of air). The computational domain is meshed with a uniform grid size of 0.16 m. In the vicinity of the free surface, the base mesh is then refined twice to obtain a finer mesh size of 0.04 m (approximately 88 steps per peak period). The grid resolution is sufficient for LES according to the criterion given in [68]. We use a time resolution of 0.01 s (approximately 150 steps per peak period) with a total simulation time of 300 s (corresponding to 160 h CPU time.) for each case. The peak period in this experiment is 1.5 s. Therefore, each time series includes 200 waves. We used a relaxation zone at the beginning of the computational domain to generate the waves and a damping zone at the end of the computational domain to absorb the waves and eliminate the impact of wave reflection on the simulation results. The parameters of the numerical simulations are shown in Table III.

First, the wind forcing generated in the numerical simulation is compared with the wind data measured in the laboratory experiment. We focus on the wind speed and turbulence intensity of the wind above the wavy surface. The wind speed very near the water surface is complex. Therefore, we only compare the wind field 80–200 mm above the free surface and describe the wind speed through the power-law wind profile. The wind speed and turbulence intensity are shown in Fig. 12(a), where the 95% confidence interval is also provided for the wind speed, and Fig. 12(b). The free-stream wind speed is set at 10 m/s. It can be seen from the wind profile in Fig. 12(a) that the wind speed near the water surface is close to the result of the laboratory experiments. The relative errors of TI, TKE, and  $\overline{\text{CTKE}}$  are typically less than approximately 10% (see Table IV). The maximum relative error of TI is 11% at  $z = 100$  mm. At  $z = 150$  mm, the maximum relative error of TKE is measured, and the value is 9.0%.  $\overline{\text{CTKE}}$  also reaches its maximum value of 12% at the same position.

As shown in Fig. 13, the results of numerical simulation are consistent with those of laboratory experiments. For case 1 NS, wind causes wave height growth. Yet, for cases 2 NS and 3 NS wind causes wave height attenuation. In the large-scale open tank, the wind has fully developed and has a high turbulence intensity.

### APPENDIX C: EXPERIMENTAL RESULTS

Here, we list the experimental results in Table V for case 1 (wave growth) and Table VI for cases 2 and 3 (for wave attenuation).

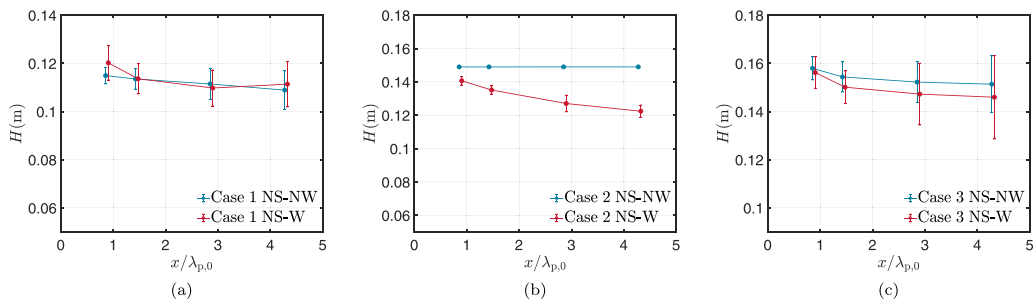


FIG. 13. Numerical results for the evolution of significant wave height with (NS-W) and without (NS-NW) wind forcing. Error bars show the 95% confidence interval based on the standard deviation.

TABLE V. Experimental results for case 1 (wave growth).

Case	Parameters	Position 1: $x/\lambda_{p,0} = 1.4$	Position 2: $x/\lambda_{p,0} = 2.8$	Position 3: $x/\lambda_{p,0} = 4.2$
Case 1 NW	$H_s$ (m)	0.1075	0.1094	0.1109
	$\varepsilon$	0.0996	0.1004	0.1007
	$\lambda_3$	0.1160	0.1369	0.1476
	$\lambda_4$	3.1891	3.1312	3.1251
	$k_p$ ( $\text{m}^{-1}$ )	1.8531	1.8370	1.8163
	$\bar{f}$ (Hz)	0.7734	0.7724	0.7729
Case 1 W	$H_s$ (m)	0.1130	0.1127	0.1146
	$\varepsilon$	0.1048	0.1040	0.1055
	$\lambda_3$	0.1294	0.1573	0.1484
	$\lambda_4$	3.2783	3.2344	3.2779
	$k_p$ ( $\text{m}^{-1}$ )	1.8547	1.8452	1.8374
	$\bar{f}$ (Hz)	0.7780	0.7865	0.7905

TABLE VI. Experimental results for case 2 and case 3 (wave attenuation).

Case	Parameters	Position 1: $x/\lambda_{p,0} = 1.4$	Position 2: $x/\lambda_{p,0} = 2.8$	Position 3: $x/\lambda_{p,0} = 4.2$
Case 2 NW	$H_s$ (m)	0.1441	0.1451	0.1449
	$\varepsilon$	0.1291	0.1304	0.1299
	$\lambda_3$	0.1835	0.2339	0.2017
	$\lambda_4$	3.3546	3.3890	3.4159
	$k_p$ ( $\text{m}^{-1}$ )	1.7925	1.7973	1.7925
	$\bar{f}$ (Hz)	0.7268	0.7265	0.7227
Case 3 NW	$H_s$ (m)	0.1581	0.1605	0.1599
	$\varepsilon$	0.1374	0.1397	0.1393
	$\lambda_3$	0.2094	0.2217	0.2154
	$\lambda_4$	3.6463	3.6588	3.6165
	$k_p$ ( $\text{m}^{-1}$ )	1.7376	1.7407	1.7423
	$\bar{f}$ (Hz)	0.7030	0.7023	0.7026
Case 2 W	$H_s$ (m)	0.1223	0.1215	0.1239
	$\varepsilon$	0.1110	0.1105	0.1130
	$\lambda_3$	0.1485	0.1614	0.1836
	$\lambda_4$	3.5443	3.6628	3.7267
	$k_p$ ( $\text{m}^{-1}$ )	1.8147	1.8179	1.8243
	$\bar{f}$ (Hz)	0.7487	0.7590	0.7699
Case 3 W	$H_s$ (m)	0.1435	0.1421	0.1419
	$\varepsilon$	0.1299	0.1280	0.1281
	$\lambda_3$	0.1858	0.2040	0.2008
	$\lambda_4$	3.8661	3.8662	3.8788
	$k_p$ ( $\text{m}^{-1}$ )	1.8099	1.80220	1.8052
	$\bar{f}$ (Hz)	0.7275	0.7336	0.7352

- [1] L. Ma and C. Swan, An experimental study of wave-in-deck loading and its dependence on the properties of the incident waves, *J. Fluids Struct.* **92**, 102784 (2020).
- [2] K. Dysthe, H. E. Krogstad, and P. Müller, Oceanic rogue waves, *Annu. Rev. Fluid Mech.* **40**, 287 (2008).
- [3] G. Lawton, Monsters of the deep, *New Sci.* **170**, 28 (2001).
- [4] P. C. Liu, A chronology of freak wave encounters, *Geofizika* **24**, 57 (2007).
- [5] M. Onorato, S. Residori, U. Bortolozzo, A. Montina, and F. Arecchi, Rogue waves and their generating mechanisms in different physical contexts, *Phys. Rep.* **528**, 47 (2013).
- [6] C. Kharif and E. Pelinovsky, Physical mechanisms of the rogue wave phenomenon, *Eur. J. Mech. B: Fluids* **22**, 603 (2003).
- [7] G. Ducrozet, M. Abdolahpour, F. Nelli, and A. Toffoli, Predicting the occurrence of rogue waves in the presence of opposing currents with a high-order spectral method, *Phys. Rev. Fluids* **6**, 064803 (2021).
- [8] T. B. Benjamin and J. E. Feir, The disintegration of wave trains on deep water part 1. Theory, *J. Fluid Mech.* **27**, 417 (1967).
- [9] P. A. Janssen, Nonlinear four-wave interactions and freak waves, *J. Phys. Oceanogr.* **33**, 863 (2003).
- [10] R. Grimshaw, Two-dimensional modulation instability of wind waves, *J. Ocean Eng. Mar. Energy* **5**, 413 (2019).
- [11] Y. Xu and X. Yu, Enhanced atmospheric wave boundary layer model for evaluation of wind stress over waters of finite depth, *Prog. Oceanogr.* **198**, 102664 (2021).
- [12] X. Chen, Z. Jiang, Q. Li, Y. Li, and N. Ren, Extended environmental contour methods for long-term extreme response analysis of offshore wind turbines, *J. Offshore Mech. Arct. Eng. Trans. ASME* **142**, 052003 (2020).
- [13] Z. Li, K. Ghia, Y. Li, Z. Fan, and L. Shen, Unsteady Reynolds-averaged Navier–Stokes investigation of free surface wave impact on tidal turbine wake, *Proc. R. Soc. A* **477**, 20200703 (2021).
- [14] L. Zhang, Y. Li, W. Xu, Z. Gao, L. Fang, R. Li, B. Ding, B. Zhao, J. Leng, and F. He, Systematic analysis of performance and cost of two floating offshore wind turbines with significant interactions, *Appl. Energy* **321**, 119341 (2022).
- [15] R. Claus and M. López, Key issues in the design of floating photovoltaic structures for the marine environment, *Renewable Sustainable Energy Rev.* **164**, 112502 (2022).
- [16] D. Keiner, O. Salcedo-Puerto, E. Immonen, W. G. van Sark, Y. Nizam, F. Shadiya, J. Duval, T. Delahaye, A. Gulagi, and C. Breyer, Powering an island energy system by offshore floating technologies towards 100 renewables: A case for the Maldives, *Appl. Energy* **308**, 118360 (2022).
- [17] W. Liu, S. Chen, K. Hu, X. Guo, Q. Wang, X. Song, Z. Liu, and Y. Li, Experimental and numerical investigation of the hydroelastic response of a hinged hexagon enclosed platform in waves, *IEEE J. Ocean. Eng.* **49**, 368 (2023).
- [18] I. B. Savelyev, B. K. Haus, and M. A. Donelan, Experimental study on wind-wave momentum flux in strongly forced conditions, *J. Phys. Oceanogr.* **41**, 1328 (2011).
- [19] M. Onorato and D. Proment, Approximate rogue wave solutions of the forced and damped nonlinear Schrödinger equation for water waves, *Phys. Lett. A* **376**, 3057 (2012).
- [20] M. Brunetti and J. Kasparian, Modulational instability in wind-forced waves, *Phys. Lett. A* **378**, 3626 (2014).
- [21] M. Maleewong and R. Grimshaw, Evolution of water wave groups with wind action, *J. Fluid Mech.* **947**, A35 (2022).
- [22] A. Chabchoub, N. Hoffmann, H. Branger, C. Kharif, and N. Akhmediev, Experiments on wind-perturbed rogue wave hydrodynamics using the peregrine breather model, *Phys. Fluids* **25**, 101704 (2013).
- [23] A. Toffoli, A. Alberello, H. Clarke, F. Nelli, A. Benetazzo, F. Bergamasco, B. N. Ntamba, M. Vichi, and M. Onorato, Observations of rogue seas in the southern ocean, *Phys. Rev. Lett.* **132**, 154101 (2024).
- [24] W. Peirson, A. Garcia, and S. Pells, Water wave attenuation due to opposing wind, *J. Fluid Mech.* **487**, 345 (2003).
- [25] J. Touboul, J. P. Giovanangeli, C. Kharif, and E. Pelinovsky, Freak waves under the action of wind: Experiments and simulations, *Eur. J. Mech. B: Fluids* **25**, 662 (2006).
- [26] C. Kharif, J. P. Giovanangeli, J. Touboul, L. Grare, and E. Pelinovsky, Influence of wind on extreme wave events: Experimental and numerical approaches, *J. Fluid Mech.* **594**, 209 (2008).

- [27] Z. Tian and W. Choi, Evolution of deep-water waves under wind forcing and wave breaking effects: Numerical simulations and experimental assessment, *Eur. J. Mech. B: Fluids* **41**, 11 (2013).
- [28] A. Saket, W. Peirson, M. Banner, X. Barthelemy, and M. Allis, On the threshold for wave breaking of two-dimensional deep water wave groups in the absence and presence of wind, *J. Fluid Mech.* **811**, 642 (2017).
- [29] Q. Zou and H. Chen, Wind and current effects on extreme wave formation and breaking, *J. Phys. Oceanogr.* **47**, 1817 (2017).
- [30] J. Wang, S. Yan, and Q. Ma, Deterministic numerical modelling of three-dimensional rogue waves on large scale with presence of wind, *Proc. IUTAM* **26**, 214 (2018).
- [31] S. Hasan, V. Sriram, and P. Selvam, Numerical modelling of wind-modified focused waves in a numerical wave tank, *Ocean Eng.* **160**, 276 (2018).
- [32] T. Cao, B. Deng, and L. Shen, A simulation-based mechanistic study of turbulent wind blowing over opposing water waves, *J. Fluid Mech.* **901**, A27 (2020).
- [33] J. H. Lee and J. P. Monty, On the interaction between wind stress and waves: Wave growth and statistical properties of large waves, *J. Phys. Oceanogr.* **50**, 383 (2020).
- [34] T. Cao and L. Shen, A numerical and theoretical study of wind over fast-propagating water waves, *J. Fluid Mech.* **919**, A38 (2021).
- [35] L. Shemer and S. K. Singh, Spatially evolving regular water wave under the action of steady wind forcing, *Phys. Rev. Fluids* **6**, 034802 (2021).
- [36] J. Kristoffersen, H. Bredmose, C. Georgakis, H. Branger, and C. Luneau, Experimental study of the effect of wind above irregular waves on the wave-induced load statistics, *Coast. Eng.* **168**, 103940 (2021).
- [37] N. Husain, T. Hara, and P. Sullivan, Wind turbulence over misaligned surface waves and air-sea momentum flux. Part I: Waves following and opposing wind, *J. Phys. Oceanogr.* **52**, 119 (2021).
- [38] G. Deskos, S. Ananthan, and M. Sprague, Direct numerical simulations of turbulent flow over misaligned traveling waves, *Int. J. Heat Fluid Flow* **97**, 109029 (2022).
- [39] H. Chen and Q. Zou, Geometry of deep and intermediate water breaking waves influenced by wind speed and direction, *Phys. Fluids* **34**, 087126 (2022).
- [40] N. Husain, T. Hara, and P. Sullivan, Wind turbulence over misaligned surface waves and air-sea momentum flux. Part II: Waves in oblique wind, *J. Phys. Oceanogr.* **52**, 141 (2021).
- [41] J. Touboul, On the influence of wind on extreme wave events, *Nat. Hazards Earth Syst. Sci.* **7**, 123 (2007).
- [42] J. Touboul, C. Kharif, E. Pelinovsky, and J. P. Giovanangeli, On the interaction of wind and steep gravity wave groups using Miles' and Jeffreys' mechanisms, *Nonlin. Processes Geophys.* **15**, 1023 (2008).
- [43] T. Waseda and M. P. Tulin, Experimental study of the stability of deep-water wave trains including wind effects, *J. Fluid Mech.* **401**, 55 (1999).
- [44] A. Toffoli, D. Proment, H. Salman, J. Monbaliu, F. Frascoli, M. Dafilis, E. Stramignoni, R. Forza, M. Manfrin, and M. Onorato, Wind generated rogue waves in an annular wave flume, *Phys. Rev. Lett.* **118**, 144503 (2017).
- [45] T. A. A. Adcock and P. H. Taylor, Energy input amplifies nonlinear dynamics of deep water wave groups, *Int. J. Offshore Polar Eng.* **21**, 8 (2011).
- [46] X. Hao and L. Shen, Large-eddy simulation of gusty wind turbulence over a travelling wave, *J. Fluid Mech.* **946**, A8 (2022).
- [47] J. Garratt, Review: The atmospheric boundary layer, *Earth-Sci. Rev.* **37**, 89 (1994).
- [48] A. Viselli, N. Faessler, and M. Filippelli, Lidar measurements of wind shear exponents and turbulence intensity offshore the northeast united states, *J. Offshore Mech. Arctic Eng.* **144**, 042001 (2022).
- [49] S. Caires, J.-J. Schouten, L. Lønseth, V. Neshaug, I. Pathirana, and O. Storås, Uncertainties in offshore wind turbulence intensity, *J. Phys.: Conf. Ser.* **1356**, 012037 (2019).
- [50] M. Onorato, A. R. Osborne, M. Serio, L. Cavaleri, C. Brandini, and C. T. Stansberg, Observation of strongly non-Gaussian statistics for random sea surface gravity waves in wave flume experiments, *Phys. Rev. E* **70**, 067302 (2004).
- [51] T. Tang, W. Xu, D. Barratt, H. B. Bingham, Y. Li, P. H. Taylor, T. S. van den Bremer, and T. A. A. Adcock, Spatial evolution of the kurtosis of steep unidirectional random waves, *J. Fluid Mech.* **908**, A3 (2021).

- [52] Y. Liu, D. Eeltink, T. Tang, D. Barratt, Y. Li, T. A. A. Adcock, and T. S. van den Bremer, Comparison of breaking models in envelope-based surface gravity wave evolution equations, *Phys. Rev. Fluids* **8**, 054803 (2023).
- [53] Z. Zhang, T. Tang, and Y. Li, Spatial estimation of unidirectional wave evolution based on ensemble data assimilation, *Eur. J. Mech. B: Fluids* **106**, 1 (2024).
- [54] M. A. Serio, M. A. Onorato, A. Osborne, and P. Janssen, On the computation of the Benjamin-Feir index, *Nuovo Cimento Soc. Ital. Fis., C* **28**, 893 (2005).
- [55] Y. Goda, *Random Seas and Design of Maritime Structures* (World Scientific, Singapore, 2000).
- [56] C. Prasada Rao, Spectral width parameter for wind-generated ocean waves, *Proc. Indian Acad. Sci.* **97**, 173 (1988).
- [57] M. Onorato, L. Cavaleri, S. Fouques, O. Gramstad, P. A. E. M. Janssen, J. Monbaliu, A. R. Osborne, C. Packozdi, M. Serio, C. T. Stansberg, A. Toffoli, and K. Trulsen, Statistical properties of mechanically generated surface gravity waves: A laboratory experiment in a three-dimensional wave basin, *J. Fluid Mech.* **627**, 235 (2009).
- [58] M. Onorato, A. R. Osborne, M. Serio, L. Cavaleri, C. Brandini, and C. T. Stansberg, Extreme waves, modulational instability and second order theory: Wave flume experiments on irregular waves, *Eur. J. Mech. B: Fluids* **25**, 586 (2006).
- [59] T. Hara and C. C. Mei, Frequency downshift in narrowbanded surface waves under the influence of wind, *J. Fluid Mech.* **230**, 429 (1991).
- [60] M. Tayfun, Narrow-band nonlinear sea waves, *J. Geophys. Res.* **85**, 1548 (1980).
- [61] G. Z. Forristall, Wave crest distributions: Observations and second-order theory, *J. Phys. Oceanogr.* **30**, 1931 (2000).
- [62] T. Zdyski and F. Feddersen, Wind-induced changes to surface gravity wave shape in deep to intermediate water, *J. Fluid Mech.* **903**, A31 (2020).
- [63] T. Adcock and P. Taylor, Non-linear evolution of uni-directional focussed wave-groups on a deep water: A comparison of models, *Appl. Ocean Res.* **59**, 147 (2016).
- [64] M. Latheef, C. Swan, and J. Spinneken, A laboratory study of nonlinear changes in the directionality of extreme seas, *Proc. R. Soc. A* **473**, 20160290 (2017).
- [65] I. Karpadakis, C. Swan, and M. Christou, Laboratory investigation of crest height statistics in intermediate water depths, *Proc. R. Soc. A* **475**, 20190183 (2019).
- [66] S. Y. Annenkov and V. I. Shrira, Evolution of kurtosis for wind waves, *Geophys. Res. Lett.* **36**, 2009GL038613 (2009).
- [67] C. Liu, X. Li, J. Song, Z. Zou, J. Huang, J. Zhang, G. Jie, and J. Wang, Characteristics of the marine atmospheric boundary layer under the influence of ocean surface waves, *J. Phys. Oceanogr.* **52**, 1261 (2022).
- [68] H. Choi and P. Moin, Grid-point requirements for large eddy simulation: Chapman's estimates revisited, *Phys. Fluids* **24**, 011702 (2012).